PAPER • **OPEN ACCESS**

Field investigation of novel self-sensing asphalt pavement for weigh-in-motion sensing

To cite this article: Hasan Borke Birgin *et al* 2022 *Smart Mater. Struct.* **31** 085004

OPEN ACCESS
IOP Publishing
Smart Materials and Structures
Smart Mater. Struct. **31** (2022) 085004 (16pp)
https://doi.org/10.1088/1361-665X/ac7922

Field investigation of novel self-sensing asphalt pavement for weigh-in-motion sensing

Hasan Borke Birgin[1], Antonella D'Alessandro[1], Maurizio Favaro[2], Cesare Sangiorgi[3], Simon Laflamme[4] and Filippo Ubertini[1,*]

[1] University of Perugia, Department of Civil and Environment Engineering, via Goffredo Duranti 93, Perugia, Italy
[2] Padana Resine S.r.l., via Calto 731, Ceneselli (RO), Italy
[3] University of Bologna, Department of Civil, Chemical, Environmental, and Materials Engineering, via Zamboni 33, Bologna, Italy
[4] Iowa State University, Department of Civil, Construction, and Environmental Engineering, 416A Town Engr. 813 Bissell Rd., Ames, IA, United States of America

E-mail: filippo.ubertini@unipg.it

Received 3 March 2022, revised 24 April 2022
Accepted for publication 15 June 2022
Published 29 June 2022

Abstract

The integration of weigh-in-motion (WIM) sensors within highways or bridge structural health monitoring systems is becoming increasingly popular to ensure structural integrity and users safety. Compared to standard technologies, smart self-sensing materials and systems present a simpler sensing setup, a longer service life, and increased durability against environmental effects. Field deployment of such technologies requires characterization and design optimization for realistic scales. This paper presents a field investigation of the vehicle load-sensing capabilities of a newly developed low-cost, eco-friendly and high durability smart composite paving material. The novel contributions of the work include the design and installation of a full-scale sensing pavement section and of the sensing hardware and software using tailored low-cost electronics and a learning algorithm for vehicle load estimation. The outcomes of the research demonstrate the effectiveness of the proposed system for traffic monitoring of infrastructures and WIM sensing by estimating the gross weight of passing trucks within a 20% error during an autonomous sensing period of two months.

Keywords: sensing pavement, smart carbon-doped sustainable materials, field investigation, weigh-in-motion, traffic monitoring, artificial neural networks, machine learning

(Some figures may appear in colour only in the online journal)

* Author to whom any correspondence should be addressed.

1. Introduction

The ageing of infrastructure networks is a worldwide problem, with numbers of constructions requiring major maintenance having increased rapidly throughout recent years [1]. Transportation infrastructures, such as bridges, made of traditional materials, are prone to fatigue-related failures that emerge from non-standard traffic load cycles acting over long periods, which result in unexpected shorter service lives of the load-bearing elements, at the risk of sudden structural failures and collapses [2–4]. Employing fatigue life prediction models can help overcome such issues [5–8] by optimizing maintenance schedules based on real traffic conditions and actual structural performance predicted using structural health monitoring (SHM) systems [9–12].

Currently, the evaluation of the structural conditions and the prediction of the service life can be carried out by a joint assessment of structural response and traffic time history [13–15]. The structural response is commonly observed through accelerometers [16] and deformation or displacement transducers (strain gauges, LVDT's, fiber Bragg gratings) [17–19], placed at strategic locations [20]. More recently, visual procedures and systems with increasing accuracy and measurement nodes have been developed [21–24].

However, in general, specific aspects limit the long-term deployment of autonomous monitoring systems. First, accurate and low-noise sensors are expensive, and the sensing performance depends on the quality of labor during the instrumentation phase [25–27]. Second, sensors can be exposed to harsh environmental conditions, decreasing their accuracy [28] and requiring frequent maintenance or replacement, thus negatively impacting the long-term stability of the SHM system [29]. Third, autonomous monitoring systems necessitate the integration of various hardware and software components, which increases their probability of failure [30].

At present, various techniques are available in the market to conduct traffic monitoring on road infrastructure. Traditional vehicle counting methods are visual, as cameras [31], or physical, through induction loops using electromagnetism [32], photoelectric sensors [33], or radio waves [34]. Considering the standard fatigue loads, the traffic volume and the occurrence frequencies of critical loads, the remaining service life of the road infrastructure can be estimated. Such an estimation depends on the standardized weights of the vehicles [35]. This estimation can be over- or under-predicting service life under actual traffic loads, thus increasing the maintenance costs or jeopardising safety, respectively.

Among available traffic load monitoring systems, the most reliable is the use of weigh-in-motion (WIM) systems [36]. These systems are used to detect and classify vehicles without interrupting the traffic flow, but require spatio-temporal readings in order to be capable of classifying vehicles appropriately [37]. The popularity of WIM systems is growing exponentially, because they have been shown to yield improved maintenance schedules, let alone their use for traffic law enforcement [38, 39]. In addition, the availability of data on traffic-structure interaction can be significant for SHM strategies [40]. Frequently used sensors in WIM systems include load cells, bending plates, and piezoelectric sensors [41, 42]. Important factors limiting the widespread deployment of WIM technologies are their limited durability, high costs, and installation difficulties [43].

To address the above-listed issues, this study proposes the field application of self-sensing smart materials as full-scale WIM systems for vehicles. To this aim, a multi-functional composite structural material is tailored, which exhibits a piezoresistive behavior through the addition of conductive carbon inclusions. The investigation of self-sensing capabilities in literature is quite diffuse for cement-based material. Possible applications of this technology are in SHM of constructions and infrastructures. In particular, intrinsic self-sensing carbon-added concrete possesses the potential to become a smart type of sensor for traffic monitoring in the forms of: embedded array of cementitious cubes doped with nickel particles [44], concrete pavement sections doped with carbon nanotubes [45], embedded cube sensor made of a cement-carbon nanotube composite [46], conductive asphalt concrete [47]. The authors developed a research campaign on self-sensing behavior cementitious materials doped with different types of carbon fillers, with applications of structural elements at large scales [48, 49]. The experience built on concretes by the authors permitted to identify the most appropriate filler, the optimal preparation procedure and the most effective electrical setup for the pavement sensor described in this paper. In particular, carbon microfibers appeared suitable for the investigated composite, and embedded copper wires were found optimal for high-scale applications.

The proposed material is highly durable and can provide accurate measurements since it is directly under contact with the loads [50]. The composite is similar to an asphalt concrete, but it is composed of a thermoplastic transparent (non-bituminous) binder (EVIzero), mixed with natural aggregates and a dope of carbon microfibers. Recent studies have found that this material has load-sensing capabilities supporting spatio-temporal measurements due to its tailored design [51]. This study inspects a full scale self-sensing smart pavement section having a width and length of 3 and 1.5 m, respectively, and a thickness of 8 cm. Such dimension represents a research leap in terms of self-sensing material scale when compared to existing literature works. Also, the utilized arrangement of the electrodes allows the sensing of traffic loads over large surface areas. The scalability of the solution combined with the data acquisition mechanism represent an important step toward field deployments of smart materials in different types of infrastructures. Here, the proposed smart pavement-based WIM system has been deployed at the factory of the EVIzero binder producer, and placed in the main service road and subject to the traffic of loaded trucks every working day. The investigated WIM system comprises the sensing pavement section, made of smart material and tailored electrical setup, an ad-hoc designed low cost DAQ hardware and a software specifically developed to carry out learning vehicle weight estimation. The novel self-sensing system is tested on the field with factory trucks over two months of autonomous sensing period, after a training period consisting of the passage of 82 trucks having known weight characteristics.

The paper is organized as follows. Section 2 discusses the sensing method including the training of the machine learning algorithm to identify vehicles weights. Section 3 describes the field investigation setup. Section 4 presents and discusses field results. Section 5 concludes the paper.

2. Smart pavement sensing system

The proposed WIM concept is illustrated in figure 1. The sensing pavement can be embedded in a section of a road or a bridge, as a normal infrastructural floor as depicted in figure 1(a).

The passage of a vehicle over the embedded pavement sensor sections made of self-sensing multi-functional composite material produces an electrical output proportional to the load magnitude. This is achieved by providing the composite material with piezoresistive properties via the incorporation of suitable carbon microfiber inclusions. The electrical response of the pavement is measured through a tailored low-cost electronics, which also powers the pavement with a very low voltage level. Load identification is carried out in a dedicated software running a learning algorithm. The electrical outputs of the sensing pavements are acquired using uniformly distributed line-type electrodes embedded within the road surface (figures 1(b) and (c)). These electrodes are used for connecting the pavement sensor to the electrical circuit of the data acquisition (figures 1(d) and (e)). Specific descriptions of the proposed WIM system are provided in the following sections.

2.1. Design of smart pavement unit

For self-sensing materials, the resistance of the pavement section between electrodes varies depending on strains induced by the axle loads applied onto the pavement surface. Figure 1(b) shows the design of the sensing pavement unit used for this field study. The pavement sensor of dimensions $300 \times 150 \times 8$ cm^3 has 12 embedded electrodes forming four groups of three electrodes which identify three sections with enough surface width to capture the passing of trucks' axles. The central electrodes of each group are placed at a distance of 30 cm. The triple electrodes of each group, at a mutual distance of 5 cm, are so arranged for redundancy against damages that may occur during the compaction phase of the smart pavement or during operations. Both ends of the embedded electrodes are connected to the data acquisition system through a tailored wires' system.

The side-view of the pavement illustrated in figure 1(c) shows the placement of the electrodes in the thickness of the self-sensing pavement. The load sensing models adopted for the electrical measurements are depicted in figures 1(d) and (e). The circuits permit to quantify the acting loads through the evaluation of the acquired voltages on the shunt resistor and on the segments of the smart pavement. These voltage readings are used for calculating the resistance time history of the self-sensing pavement section through the Ohm's law. The input voltage is 3 V DC, which is compatible with the commonly used voltage levels.

The electrical circuit in figure 1(d) is used for the initial tests on the field and the autonomous sensing of trucks during tests on the pavement. Figure 1(e) presents the alternative mode of sensing, without the shunt resistor, and with two sensing sections connected in series. The DAQ records the voltages spent through both sections which act as resistors. The voltage difference across each pavement segment is directly dependent on the electrical resistance of the pavement segment that varies scaled to the magnitude of the acting load. The difference time history, $\Psi(t)$ formulated in equation (1), of the two voltage recordings generates a load location and magnitude sensitive waveform during the pass of a vehicle.

$$\Psi(t) = \mathrm{V}_2(t) - \mathrm{V}_1(t) \tag{1}$$

where V_1 and V_2 are the voltage time histories read through pavement segments indicated in figure 1(e).

2.2. Data acquisition systems and hardware

Two DAQ systems are used in this study. The first one is a high-fidelity device used as benchmark. It consists of a National Instruments NI-PXIe-1096 chassis equipped with analog-digital converter NI-PXIe-4302 and voltage source measuring unit NI-PXIe-4138 as the DC voltage output. The equipment supplies 3 V DC voltage to the sensing circuit and simultaneously measures the voltages spent through smart pavement and the shunt resistor. The recorded voltage time histories are used to form the resistance time history of the smart pavement, $R(t)$, and the voltage difference time history between two parts of the smart pavement, $\Psi(t)$, depending on the experiment purpose. NI-PXIe-4302 is a 24-bit ADC with a high precision that can measure millivolt scales accurately. One channel of the ADC is instrumented with an analog high pass filter for measuring the high-frequency voltage time history $\mathrm{V}^{\mathrm{H}}(t)$ that is used for WIM sensing of vehicles. The filter and its circuit are shown in figure 2(a). The transfer function of the filter is given in equation (2), s being the Laplace variable, where $\mathrm{R} = 1000\ \Omega$ and $\mathrm{C} = 470\ \mu$F, resulting in a cut-off frequency of $1/(2\pi\mathrm{RC}) = 0.34$ Hz. Figure 2(b) depicts the numerically constructed bode plot of the filter, experimental values, and the cut-off frequency. The experimental values represent the amplitude of filtered sinusoidal signals having different frequencies generated by a RIGOL DG1022A function generator and read by a RIGOL DS1054 Oscilloscope.

$$\frac{\mathrm{V}_{\mathrm{out}}(s)}{\mathrm{V}_{\mathrm{in}}(s)} = \frac{s}{\frac{1}{RC} + s} \tag{2}$$

where $\mathrm{V}_{\mathrm{out}}$ and V_{in} are, high-pass filtered and unfiltered signals in Laplace space, respectively.

The second DAQ system is designed for low-cost and robust long-term sensing, allowing a possible extensive usage of the proposed smart pavement based WIM systems. The schematics illustrated in figure 3 shows the hardware parts and their related connections. Accordingly, the system consists of a Raspberry Pi Zero W [52] as the control unit, a camera, a regular 5 V USB charger, an LM2596 voltage regulator and

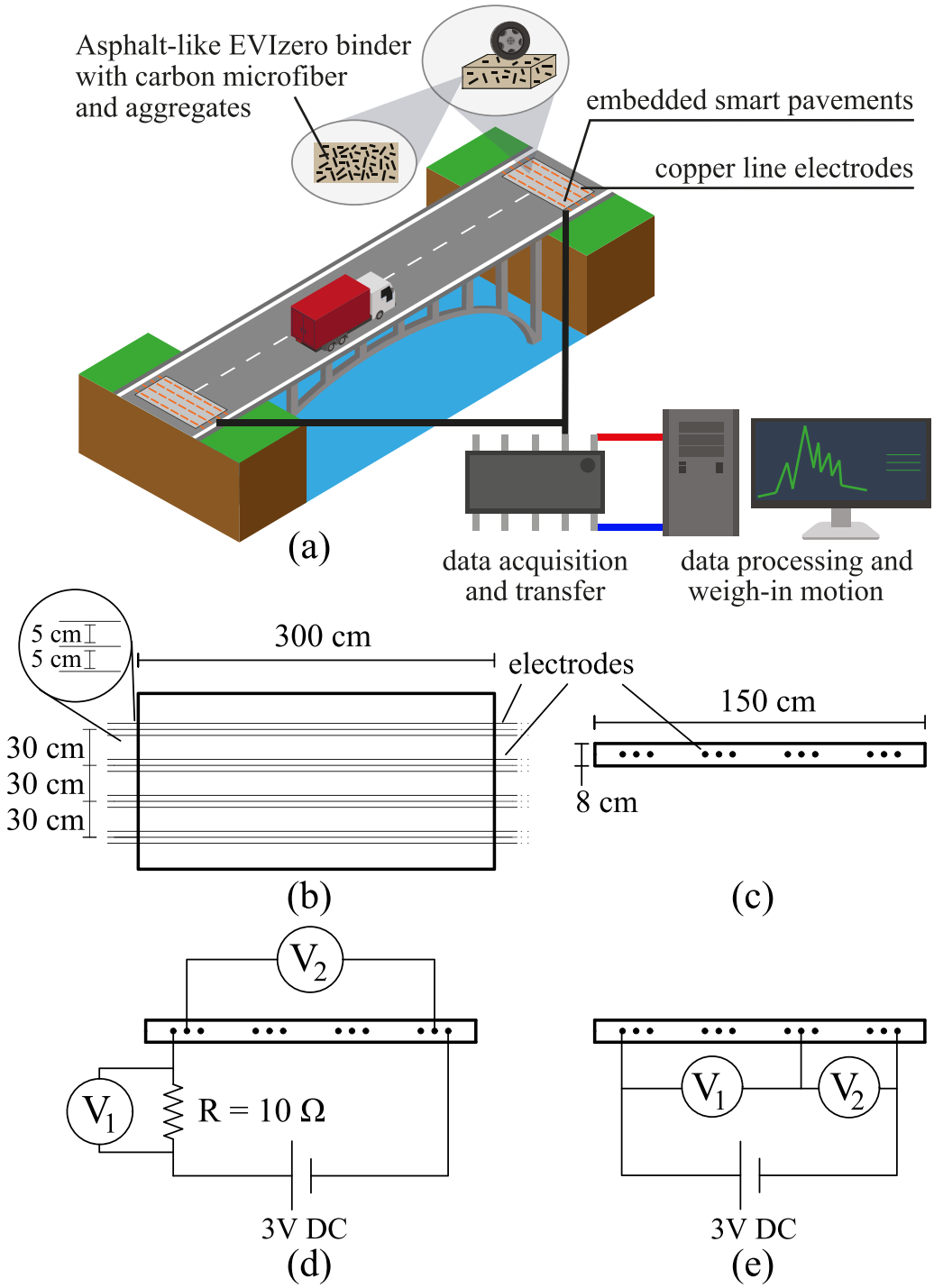

Figure 1. Concept of the WIM system: (a) illustration of the WIM sensing of road bridges system using self-sensing smart pavements; (b) top-view of the self-sensing pavement; (c) side-view of the self-sensing pavement; (d) equivalent electric circuit model that utilizes the entire pavement body as a sensor for generic load sensing; (e) equivalent electric circuit model of differential reading for wave-form signal generation.

an analog-to-digital converter, model ADS1115 [53], that is controlled by an Arduino Nano microcontroller board [54]. On the ground side, a BC549 NPN-type transistor controls the current on the circuit by functioning as an electronic switch controlled by GPIO of the Raspberry unit. The voltages through the shunt resistor and the smart pavement sensor are read using a 16-bit ADC ADS1115 by Texas Instruments. This system is developed to be online and remotely controllable. Considering current market prices at the time of the experiment, the overall cost of the developed DAQ system can be estimated as about 50 USD. The proposed data acquisition system includes components that support long operating periods, with the time limitation being the memory handling that requires periodic data transfer.

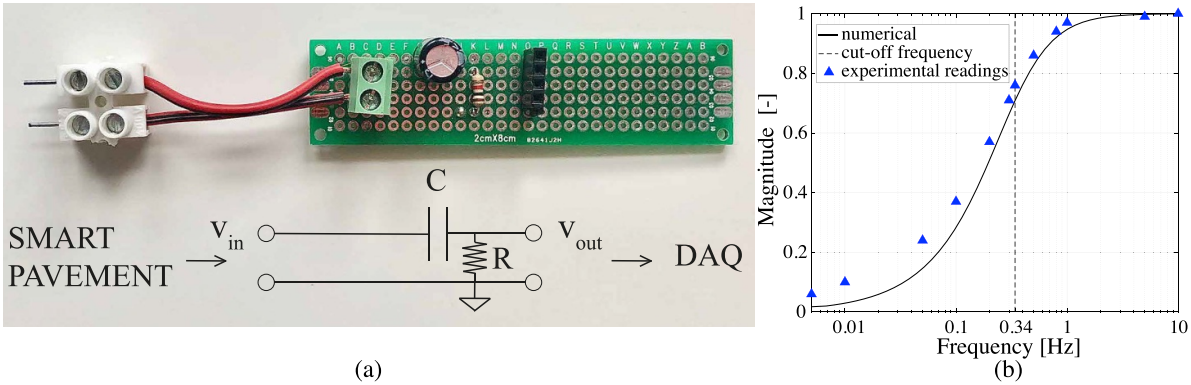

Figure 2. Passive first order RC high-pass filter employed during field WIM tests; (a) the electric circuit board and scheme; (b) plot of the passive filter together with cut-off frequency (vertical line) and experimental readings.

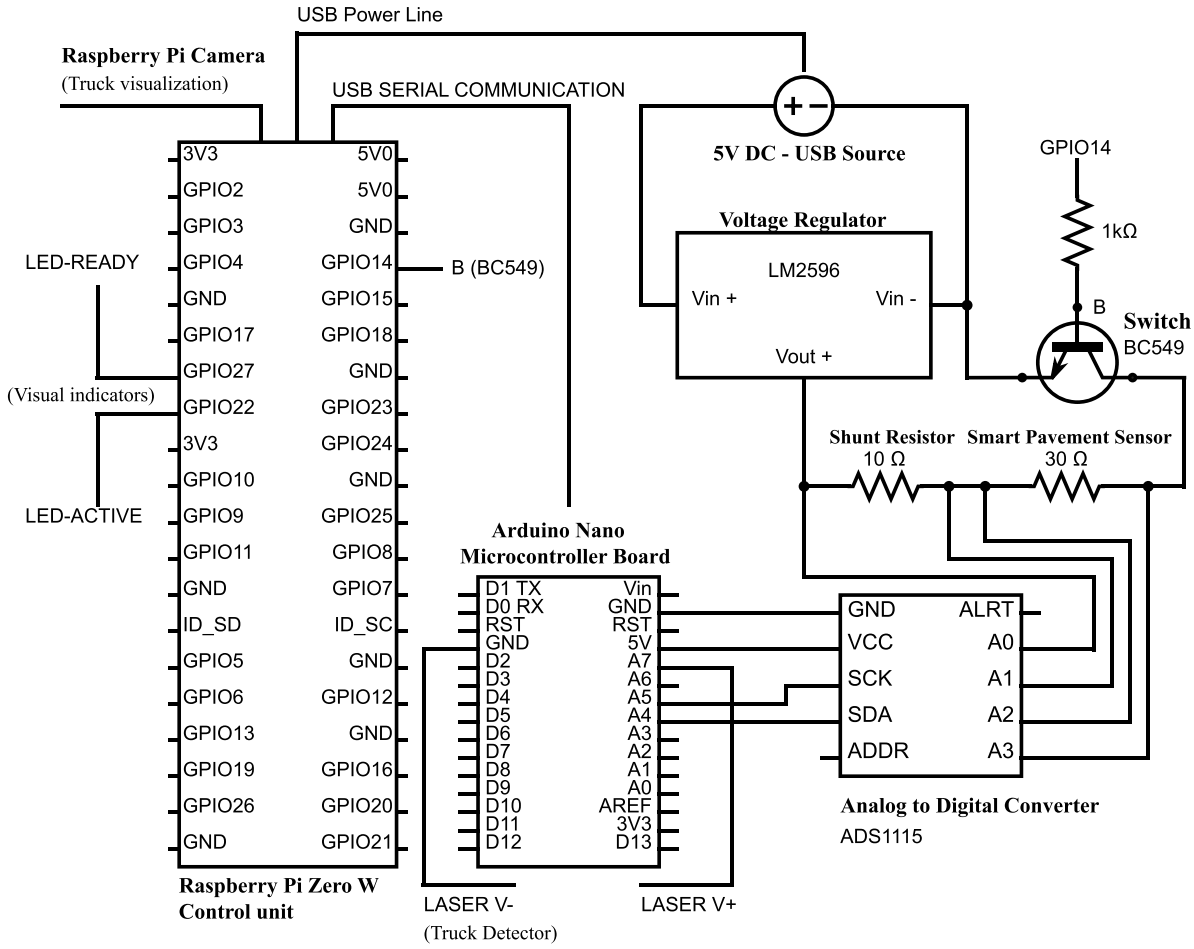

Figure 3. The hardware parts and the connection diagram of the low-cost DAQ system.

2.3. Algorithms for WIM

The WIM system investigated in this study uses three algorithms that can work individually or concurrently. The first algorithm re-creates field-measured signals during the passage of a vehicle using the data-based signal time histories with known characteristics. The process consists on the minimization problem formulated in equation (3):

$$E = \|\mathrm{V}(t) - \sum_{i=1}^{n} a_i H_i \mathrm{V}^*(t)\|_2 \tag{3}$$

where the optimization cost, E, is the Euclidian norm of the difference between the measured signal time history vector, $\mathrm{V}(t)$, and the recreated signal vector denoted by the term $\sum_{i=1}^{n} a_i H_i \mathrm{V}^*(t)$. During this operation, n stands for the total axles

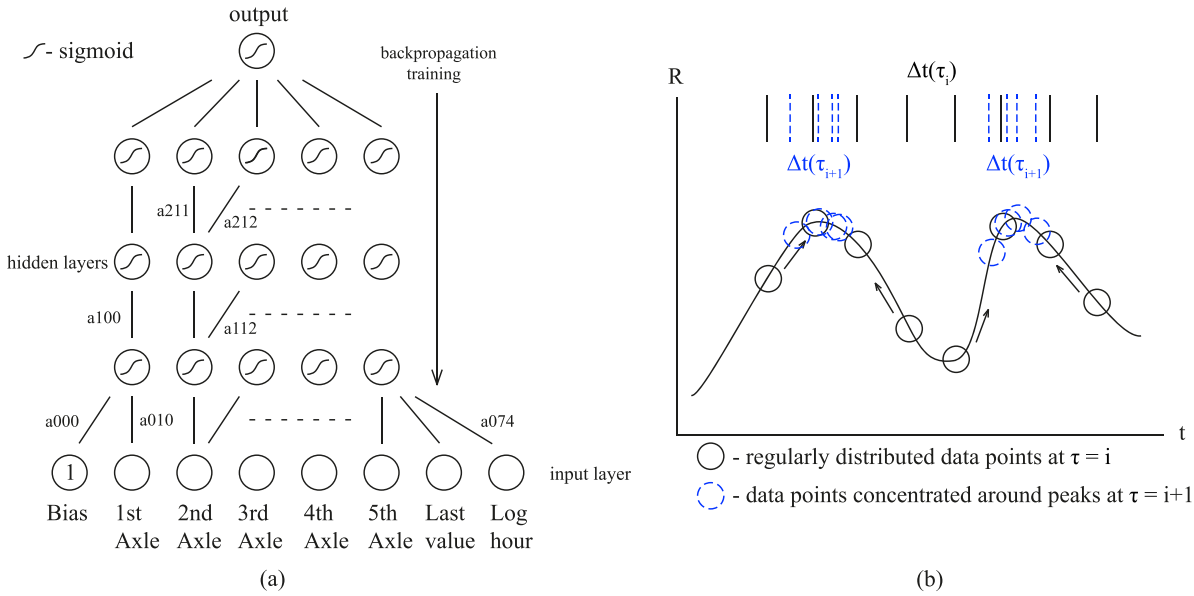

Figure 4. Algorithms used by the smart pavement: (a) the artificial neural network for weight estimation; (b) illustration of autonomous peak detection based on dynamic extremum seeking algorithm.

of the vehicle, a_i are the scaling factors, and H_i are the shifting operators in the discrete-time domain for the base signal vector $V^*(t)$, a_i and H_i are characterization variables corresponding to the weight of the axle and spacing of the axles, respectively. This methodology is explained in a previous study by the authors [37].

The second algorithm is the automated peak detection among the discrete values of a resistance time history vector created by the measurements of the self-sensing pavement, where the axle occurrences on the self-sensing pavement are detectable via the signal peaks over a resistance time history. These peaks are automatically recognizable by adapting the extremum seeking algorithm for discrete systems [55]. For this study, the extremum-seeking algorithm is employed for a statistics-based process. Initially, multiple time variables are placed evenly over the time domain of the signal recording. The resolution of time variables affects the precision and the computational demand. For this study, it is selected as 0.02 s, which is compatible with the sampling rate of the DAQ system (50 Hz) and supports the required precision according to the results. The given data acquisition rate is also compatible to vehicle speeds up to 90 km h^{-1} considering the dimensions of the sensing pavement. At the initial stage, the histogram of the time variables is uniform over the signal's time domain. Afterward, the multi-variable extremum-seeking algorithm operates until the evolution of the histogram reaches a steady state. This procedure results in autonomous detection of the time instants of signal peaks caused by the axle occurrences. The corresponding resistance values are used for the estimation of the vehicle weight.

The third algorithm is the weight estimation of passing vehicles done using deep-learning. The extracted resistance values from the recorded time histories create a training data set that serves to train a supervised artificial neural network. A neural network is designed with three layers of neurons with each layer having five neurons. The neurons contain a sigmoid kernel function defined over $\mathbb{R}$ that is introduced in equation (4), through which they can output continuous values between 0 and 1:

$$y = \frac{1}{1 + e^{-x}} \tag{4}$$

where x denotes the input to the neuron and y is the output. The artificial neural network is trained via the back-propagation algorithm [56] to output the weight estimation of the truck. Figure 4(a) illustrates the neural network architecture, where the network weights (a i-j-k) are denoted by three digits showing the layer index—source neuron index—connecting neuron index, respectively. Figure 4(b) summarizes the autonomous peak picking algorithm based on the extremum seeking, showing two distinct time instances when the data points are evenly distributed (τ_i) and being gathered to the nearest peak (τ_{i+1}).

3. Field setup and experimental campaign

3.1. Smart self-sensing pavement material

The real-scale smart pavement sensor section made of thermoplastic polymer composite self-sensing material is built and placed inside the polymer production factory of Padana Resine s.r.l. (Rovigo, Italy), on a main service road, allowing the detection of the trucks which pass frequently during the factory's regular activity. The self-sensing smart composite material is composed of a licensed commercial bitumen-like binder for road pavements called EVIzero [57], short carbon microfibers by SGL Carbon [58], and natural aggregates (aggr.). The electrodes are 3-meter long copper wires with 1 mm diameter. The mixing of the composite material is made

Table 1. Material mixture design of the self-sensing polymer composite pavement of dimensions $300 \times 150 \times 8$ cm^3, with 1% w of CMF inclusions.

Components	Aggregates			EVIzero	CMF
Size	0–4 mm	4–8 mm	8–12 mm		
Weight (kg)	225	413	112	45	0.5
Ratio to aggr. weight (%)	30	55	15	6	0.066

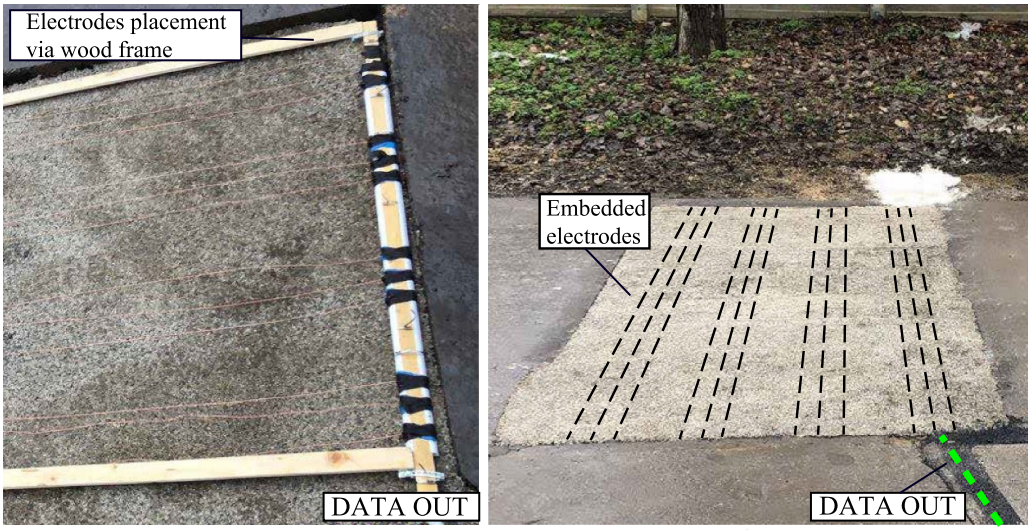

(a) (b)

Figure 5. Field implementation photos: (a) electrode holding frame, the DAQ connection is labeled 'DATA OUT'; (b) final field setup, the electrode directions are represented by black dashed lines, and the DAQ connection is displayed by a green dashed line.

mechanically at 160 °C–180 °C by a small scale rotatory hot mixer having a capacity of 600 kg. After the compaction phase, the density of the pavement is calculated approximately as 2.210 g cm^{-3}, according to the given dimensions and the weights of mix design listed in table 1. The amount of 1% w of CMF addition is based on the aspect ratio of the CMF [58] and the corresponding critical volume fraction obtained through electrical percolation model of conductive fillers, previous studies [59–61], and laboratory experiments on piezoresistivity investigating the gauge factor and linearity of the sensing model. The traffic safety performance of the investigated material, notably its anti-skid properties, is expected to be similar to that of the original pavement material due to the relatively low-concentration of CMF dispersed inside the self-sensing composite.

The electrodes are placed as shown in figure 1. In the field, the first layer of mixed material is cast and smoothed, then the electrodes are placed at desired locations by use of a wood frame, and successively the second composite layer is poured and compacted. The cooling rate of the two layers of composite material is a critical factor for the production of an uniform pavement, with optimal mechanical capacity. Figure 5(a) shows the frame adopted for the placement of the electrodes. It is formed by four wood profiles of cross-section dimension 2×1 cm^2 creating a rectangle of 120×300 cm. The copper electrodes were connected to the DAQ cables by soldering. The connections were covered by heat-resistant tapes. Figure 5(b) shows the final field installation.

3.2. Field setup

The data acquisition cabin, connected to the field electrodes is placed next to the sensing pavement. Figure 6(a) shows the dimensions of the cut on the asphalt for the placement of the self-sensing pavement. The manufactured pavement and DAQ cabin have been connected through wire ducts embedded within the roadway and embedded with cold asphalt. Figure 6(b) is a schematic of the field setup, where the main components are indicated.

The sensing system is designed to operate autonomously and capture the passing factory trucks. The following are the main steps of system procedure: (i) the laser trigger detects the passing trucks and activates the sensing trigger; (ii) the camera instantaneously captures the picture of the vehicle that triggered the laser and stores the picture for identification; (iii) the DAQ gets activated and records the data over 15 s, with a sampling rate of 50 Hz, allowing the total capture of signals generated during the passing of the trucks over the smart pavement; (iv) the data outcome and picture of the vehicle are uploaded to the cloud system for remote computing; (iv) the factory's truck scale at the end of the service road weighs the truck. This last information is used for truck identification purposes, in both training and validation phases.

The inside view of the DAQ cabin is shown in figure 7(a), where the two data acquisition systems are shown together with the remote access computer and the panel constructed by the wires attached to smart pavements' electrodes. Figure 7(b)

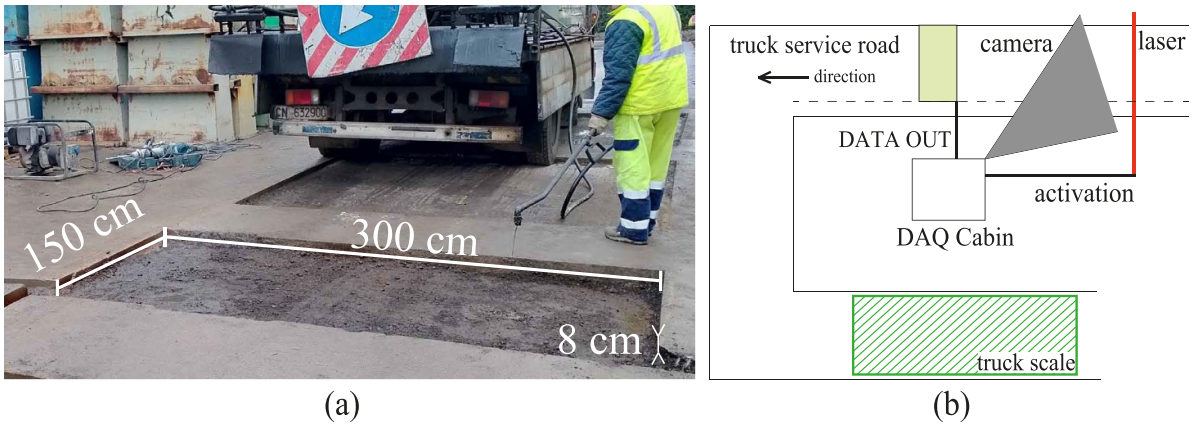

Figure 6. The self-sensing pavement settlement and the scheme of field tests; (a) the dimensions of pavement bedding and wire ducts opened on the asphalt; (b) the illustration of field scheme.

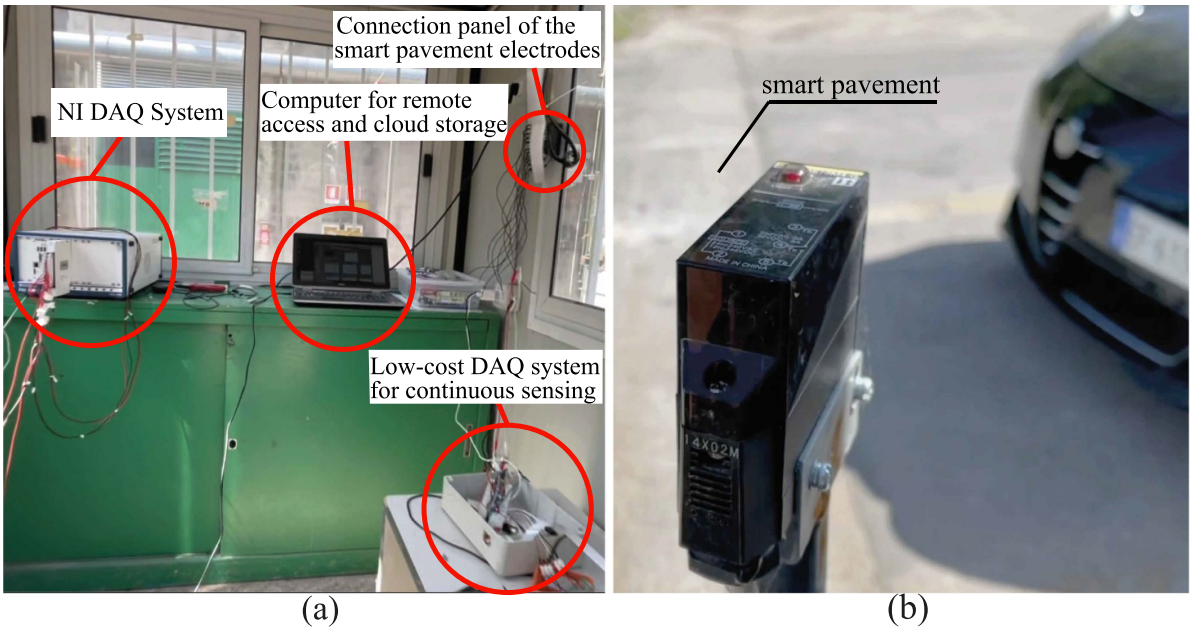

Figure 7. Devices of the field setup. (a) Inside view of the data acquisition cabin with NI-PXIe, novel DAQ, cloud computer and smart pavements connection panel; (b) the laser trigger for detection of passing vehicles.

shows the laser detector for the vehicles passing over the sensing pavement. Possible alternative methods for vehicle detection are inductive loops or visual systems, but laser trigger system is more suitable for the settlement of the study. The typical output of the designed DAQ system generated during the pass of a trailer truck is shown in figure 8, where the truck's axles are clearly visible. The presence of all peaks related to the three close-by rear axles shows the adequacy of the sensor in terms of response speed, although future research will study in depth the vehicle velocity estimation.

3.3. Experimental methodology

The field tests comprised three phases. The first phase included the preliminary verification of the pavement sensor and the theoretical WIM procedure. These tests were conducted with controllable moving loads: Car1 with a gross weight of 1800 kg, Car2 with a gross weight of 1200 kg, and the factory forklift with a gross weight of 4660 kg. The second phase concerned the tests with the factory trucks with typically five axles and different load levels: unloaded trucks weighed between 15 and 20 tons, while loaded trucks between 38 and 45 tons. A static scale inside the factory weighed the passing trucks after the test field. The third phase of the field tests was the evaluation of autonomous sensing and weight of factory trucks. That phase employed a newly developed low-cost voltage sensing and data acquisition equipment developed by the authors and tailored signal processing procedures. During this phase, 82 trucks have been recorded by the weight estimation system. The data of 12 trucks was used for validation and 70 trucks used for training of the artificial neural network. The learning has been carried out by a supervised methodology, where the estimation error was calculated based on real weights of trucks measured through static factory scale.

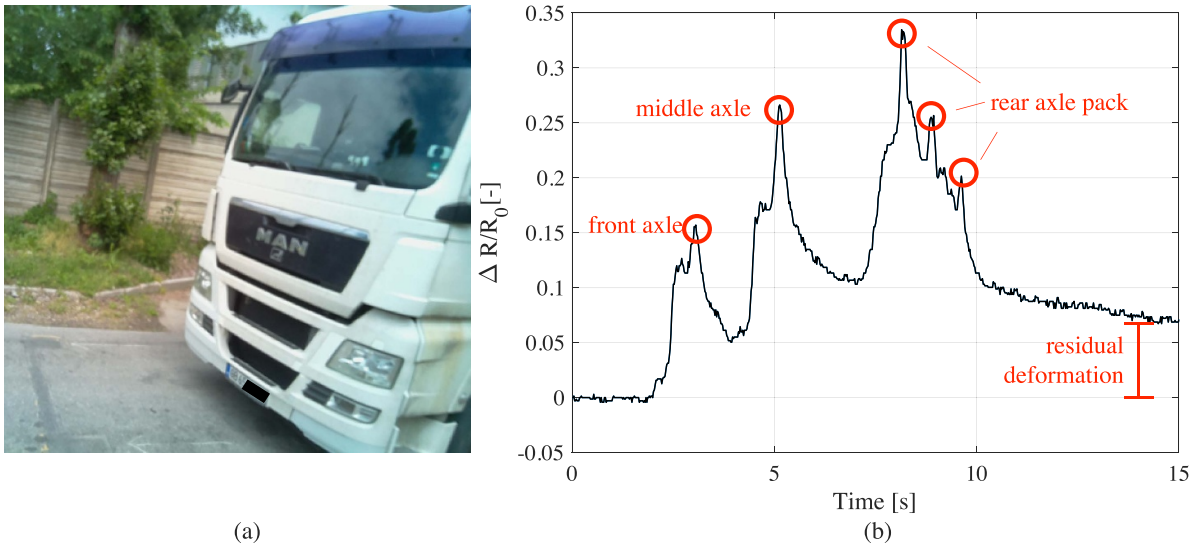

Figure 8. Typical outputs of WIM system: (a) the picture of the vehicle that triggers sensing system; (b) related variation of resistance time history together with peaks due to axle occurrences.

4. Results

4.1. Electrical characteristics

The electrical readings before the loading tests revealed the electrical characteristics of the novel pavement sensor. Recalling that the pavement included 12 line electrodes distributed inside the material, the progressive measurements of the electrical resistance between electrodes showed the growth of the resistance of pavement according to the elapsed distance to the initial electrode. The measured electrical resistance, R, can be formulated using resistivity, ρ, cross-sectional area, A, and length between electrodes, L, in the equation below which concerns a uniform rectangular shape.

$$R = \rho \frac{L}{A}. \tag{5}$$

The cross-sectional area of the segments between electrodes (A) was 2400 cm^{-2}, while the elapsed length (L) used the initial electrode as the zero-reference. The growth of electrical resistance was inspected by plotting the resistance readings between different electrodes, as depicted in figure 9.

The obtained results reflected the consistency with the linear growth model of resistance through the pavement, and confirmed that the surrounding asphalt did not affect the electrical conduction of the pavement sensor. Using the established resistance model and the results of electrical readings, the resistivity of the pavement sensor was evaluated as $\rho =$ 236.4 Ω cm. Based on the same model, the total resistance of the DAQ wires was found to be approximately equal to 5 Ω. The electrical readings confirmed one-directional current flow inside the pavement under the specific boundary conditions. This conclusion also indicated a homogeneous dispersion of carbon fibers, therefore implying the reliability of the pavement sensor for the upcoming vehicle measurements.

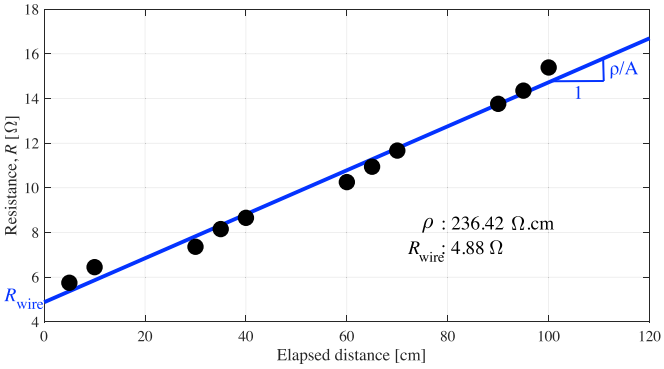

Figure 9. Linear resistance growth model with respect to the distance from the starting electrode. The resistance readings between the starting and specified electrodes are shown by circles, and the linear fit line of the resistance model is depicted in blue.

4.2. Preliminary testing of sensing principles

The preliminary tests have been conducted to verify that the pavement sensor generated signal responses scalable to the different vehicle weights and repeatable. To test the scalability of responses, three types of vehicles with different weights described in the previous section crossed over the pavement. The data generated by the pavement sensor is depicted in figure 10(a). Accordingly, two observable peaks coinciding with the axles were generated by the pavement during the vehicles passes. The results evidenced two peculiarities. First, the summation of the amplitudes of the peaks is proportional to the gross weights of the passing vehicles. Figure 10(b) shows the linearity of the results. Second, the weight variation between the front and rear axles of each vehicle, depending on the presence of the engine, is also recognizable in the graphs.

The repeatability of the pavement's response was examined through subsequent forward-backward passes of vehicles Car1

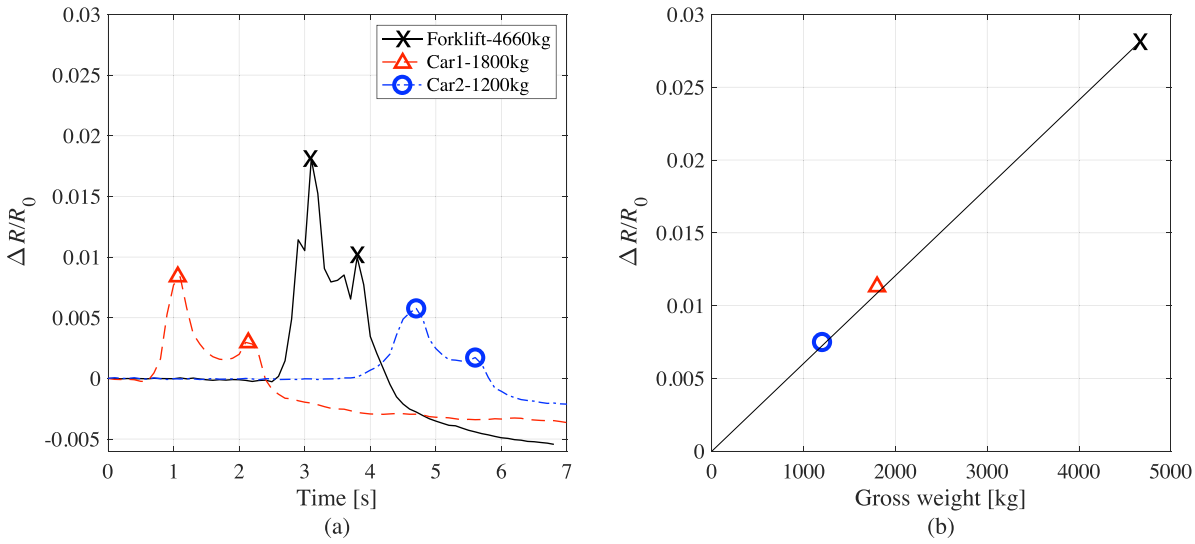

Figure 10. Passes of three different vehicles and related signal responses in terms of fractional variation of resistance time history: (a) generated signals; (b) established linear model by summation of the peak values achieved by both axles of vehicles.

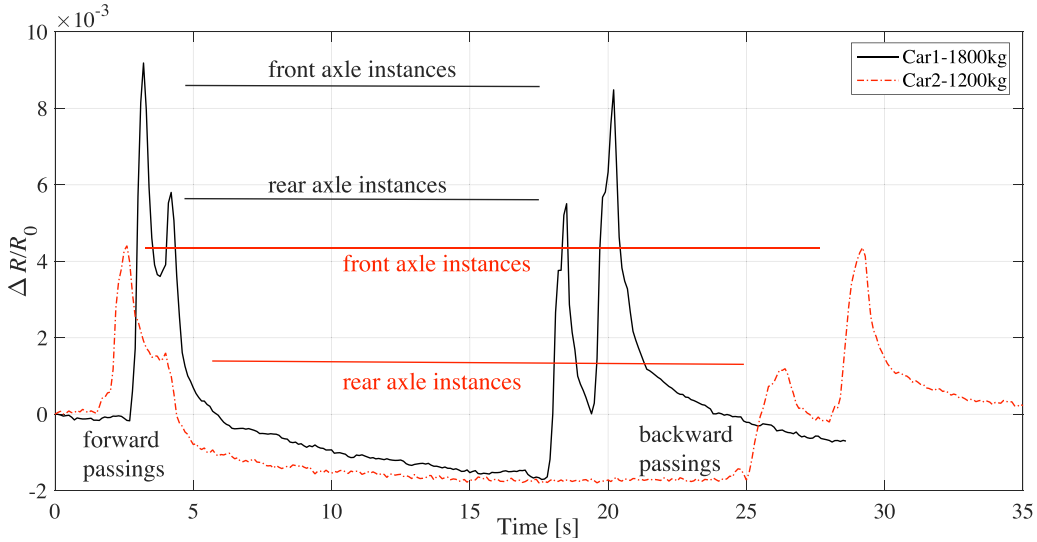

Figure 11. Fractional variation of resistance time history for forward and backward passes of two different types of vehicle, namely Cars1 and Cars2.

and Car2. The aim of this test was to show that the pavement's response to axle weights is consistent and independent of vehicles' direction. Figure 11 depicts the two-time histories recorded during the test.

Similar to the previous test results, the peak magnitudes appear scalable to the vehicle gross weights and axles' weights. In addition, the peaks detected in the forward and backward vehicles' directions are very similar, thus demonstrating the reliability of the outputs.

4.3. Wave form shaped-time histories for the WIM characterization algorithm

The sensing circuit of the pavement sensor has been configured as in figure 1(e). As discussed in the previous sections, the measurements under this configuration generate WIM compatible signals that exhibit spatio-temporal outcomes. In this section the behavior of the sensor is further investigated. Car2 passed over the sensing pavement in the following patterns: (i) forward pass repeated twice, (ii) backward pass repeated twice, (iii) front axle passes subsequently backward and forward. The read signal time histories are shown in figure 12.

The signal responses indicate that pavement sensor generated repetitive signals with similar characteristics. However, the viscoelastic nature of the pavement material increased the recovery time of the pavement after the passing load, thus affecting the outcomes by causing residual drifts. This residual effects are more evident when inspecting the first passes of vehicles in figures 12(a) and (b), where the smart pavement sensor was in a relaxed initial state.

An improved operation including the signal reconstruction according to equation (3) was carried out by employing an analog first-order passive RC high-pass filter connected between

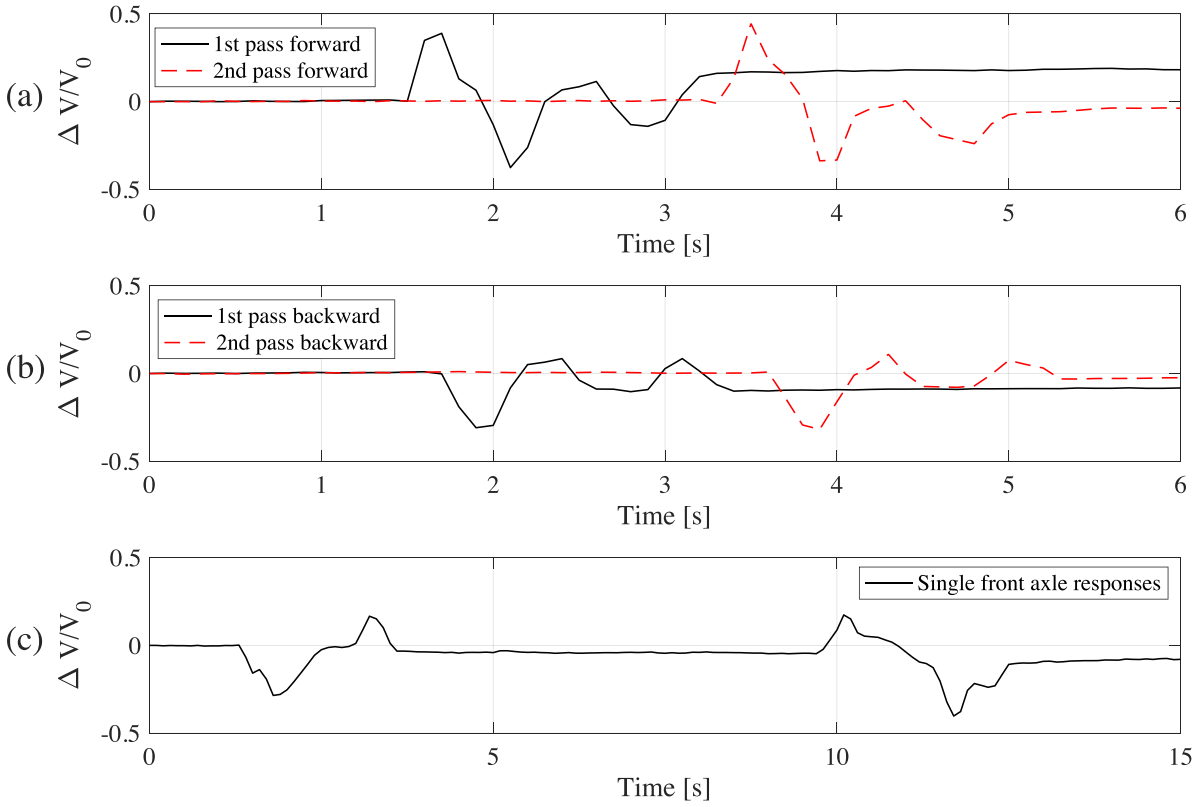

Figure 12. The results of wave-form signal production using Car2 in terms of normalized voltage time history reading: (a) forwards pass performed twice; (b) backward pass performed twice; (c) consequent backward and forward passes of the front axle, respectively.

the pavement sensor and the data acquisition system. Using the high-pass filter, the slow recovery effects were removed from the recorded time history. During the field tests, the time history readings obtained through the high-pass filtered channel of the NI-PXIe data acquisition system were used as WIM signals. These readings are denoted by $V^H(t)$. Car2 was used to generate the aforementioned high-frequency signals shown in figure 13(a), where the passing sequences are given as follows: (i) forward pass, (ii) backward pass, (iii) front-axle-only forward pass, (iv) rear-axle-only forward pass, (v) rear-axle-only backward pass, (vi) front-axle-only backward pass. The goal is to reproduce the pavement's signal response to forward and backward passes of Car2 by shifting and superposing the signal outcome of individual axles as shown in figure 13(b).

Figures 13(c) and (d) plotted the reproductions of the pavement-generated signal outcomes during the passing of Car2 by superposing the individual axle responses as hypothesized by the WIM characterization algorithm described in [37]. These results represent the first field verifications of the WIM characterization algorithm developed for self-sensing smart pavement sensors.

4.4. Records of 5-axle trucks

For investigating the sensing field properties of the developed pavement sensor system for higher loads, important for the detection of imposed excessive loads on the road infrastructures, 5-axle trailer trucks have been used as passing vehicles. The trucks passed at a steady speed over the pavement sensor. Right after, the truck scale at the end of the factory service road measured the weights of the vehicles. Figure 14(a) depicts the pavement-generated signals induced by the 5-axle trucks at different load states: loaded or unloaded, depending on their operation schedule.

The measured signals include 5-peaks in the time history that map the 5-axle configurations of the trailer trucks. Moreover, the axle-induced resistance variations show consistency with the load states of the trucks. The signals also reflect the distances between the five axles. Another significant remark is the weight distribution over the axles. In the unloaded state, the front axle bears more portion of the gross weight of the truck due to the front located motor. Once the trucks are loaded, the second axle of the trucks becomes more critical, while the last three axles have an individually smaller portion of the weight on them due to being close-coupled. Figure 14(b) depicts the data set created by the peak values of resistance variations. On this three-dimensional plot, each dot corresponds to a truck, where their load state is defined by having the red (loaded) or black (unloaded) color. The x-axis represents the values obtained during the passage of the first axle. The values at the passage of the second axle are shown in the y-axis. The summations of values encountered at the passing of the last three axles are plotted in the z-axis. A basic categorization according to the gross weights of trucks with a threshold of 20 tons is demonstrated. Accordingly, two weight classes appear distinctive, and a classification based on

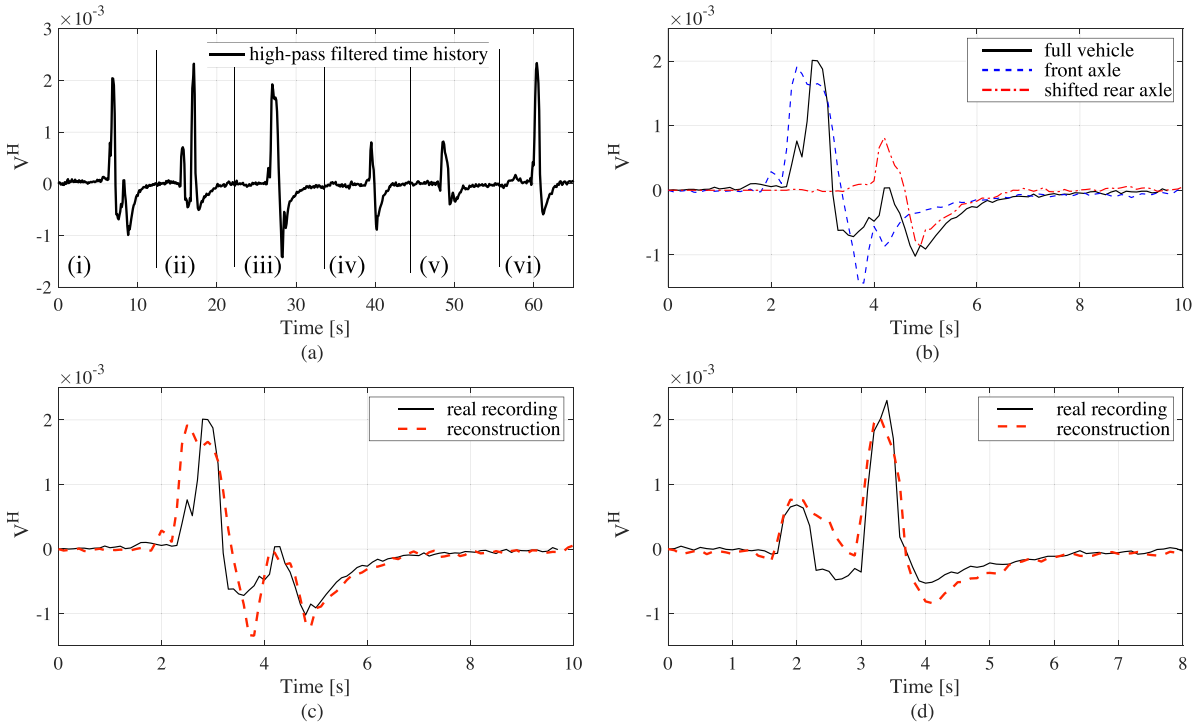

Figure 13. Signal reconstruction tests carried out with Car2 by shifting and superposition of high-pass filtered signals according to the WIM algorithm; (a) the full sequence; (b) the shifted basis signals; (c) reconstructed forward pass; (d) reconstructed backward pass.

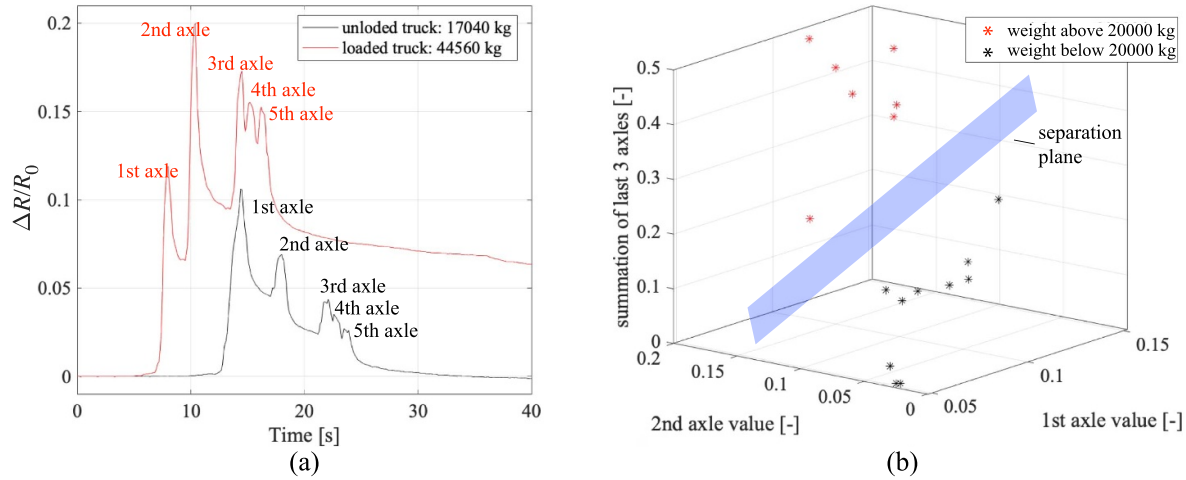

Figure 14. Data generated by truck passes. (a) Typical signals obtained from trucks under loaded and unloaded states; (b) mapped peak values from axle passes and the categorization based on a 20 000 kg threshold. The summation of the values from the last three axles are indicated in the z-coordinate.

these outcomes is found appropriate for autonomous decision systems.

4.5. Low-cost data acquisition system and autonomous weight estimation

The low-cost task oriented sensing and data acquisition system shown in figure 3 has operated during the period of February–March 2021. After the sensing period, no material deformation or damage to the sensing pavement have been visually observed. Based on collected data, weight estimations of continuously passing trucks by using the artificial neural network methodology presented in section 2.3 have been conducted. A total of 82 trucks have been recorded by the self-sensing pavement and then measured by the truck scale. The typical signal output presented in figure 8(b) shows six values existing to be used for weight estimation. Five of them are the peak values corresponding to the axles occurrences, and the sixth value is the last value of the time history recorded through the data acquisition, which reflects the measure for the residual deformation of the smart pavement. The neural network presented in figure 4(a) has a seventh input for doing

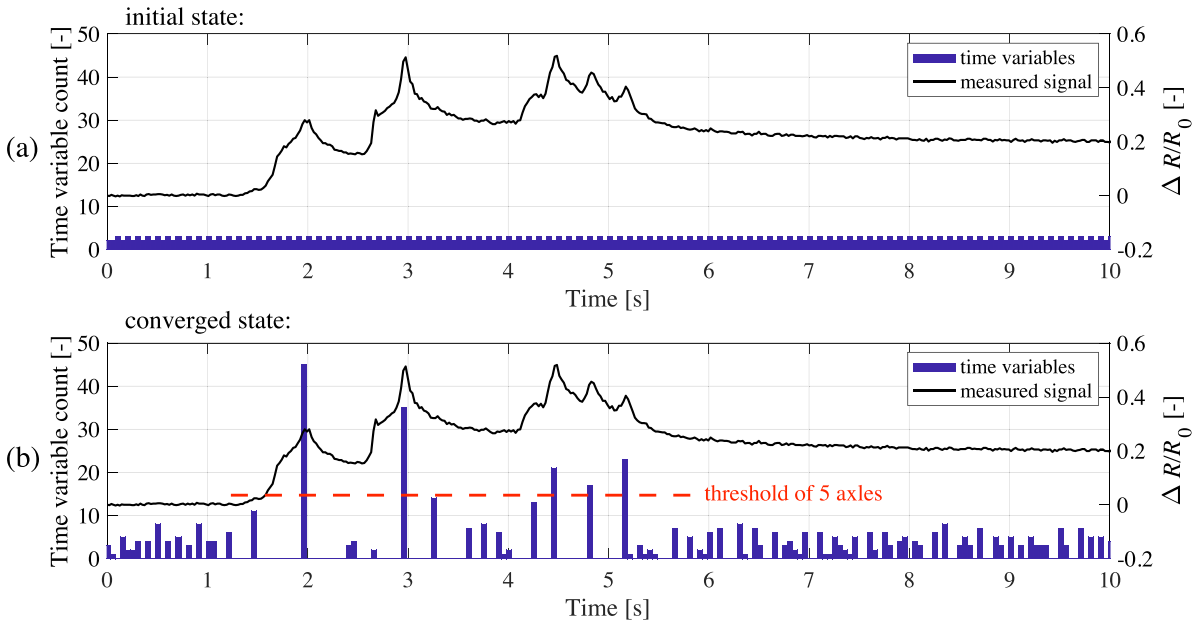

Figure 15. Initial and converged histograms created from the distributions of time variables during the operation of the autonomous peak-picking algorithm. The five time instances above the dashed red line denote the time occurrences of five axles of the factory truck.

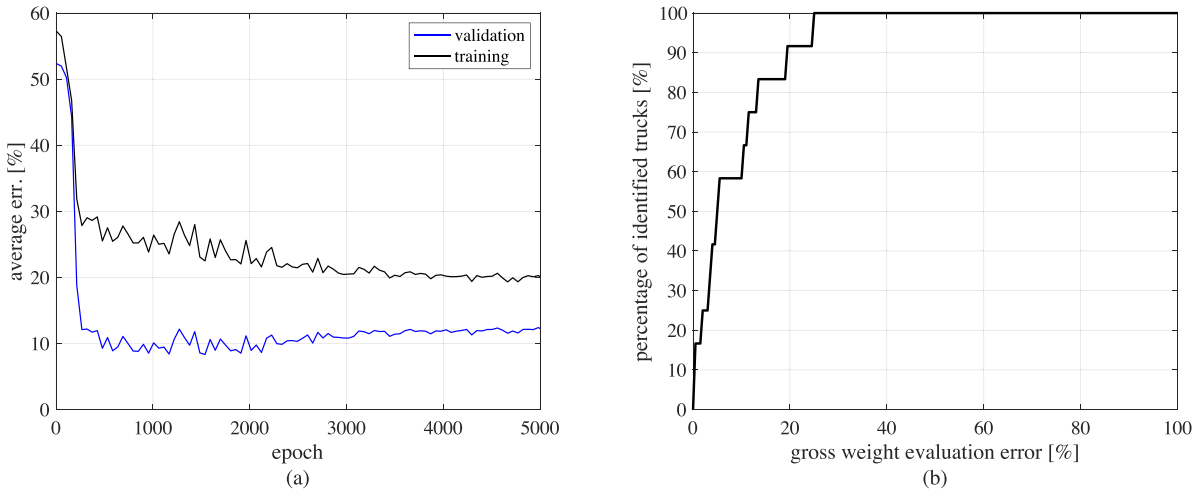

Figure 16. Autonomous weight estimation results of trucks based on data acquired by low-cost electronics system: (a) the learning curves of artificial neural network; (b) the weight estimation performance evolution according to desired error levels.

a weight estimation that is in addition to the six values coming from the recorded signals: the hour information of the log file that compensates for the ambient temperature difference during day time. The weight estimation procedure operates autonomously. Figures 15(a) and (b) plot the histograms of initial and converged states of the peak-picking algorithm, respectively. Accordingly, after the algorithm converges, the five time instances of axle occurrences coincide with the time windows that contain the five most data points within these occurrences are visually separated from the rest by a dashed red line.

The data of randomly selected 12 out of 82 trucks forms the validation set, and the remaining data constitutes the training set. The values in the data set are normalized to have values between 0 and 1, where, in terms of gross weight, the value 1 corresponds to the maximum gross weight encountered in the whole data set that includes training and validation sets. Likewise, in terms of the hour of the day, the value 24 corresponds to the value of 1 after normalization. Figure 16 reports the weight estimation outcomes.

Figure 16(a) shows the convergence of the back-propagation algorithm. The error trends over the training epoch have the anticipated evolution for both the validation set and training set. Figure 16(b) shows the performance of the developed weight estimation procedure for different desired error levels. Accordingly, the results demonstrate that the weights of 90% of the trucks in the validation set are identified with less than 20% error, which is the maximum error limit defined by the international standards. The real weights of trucks of the validation set and their estimations are given

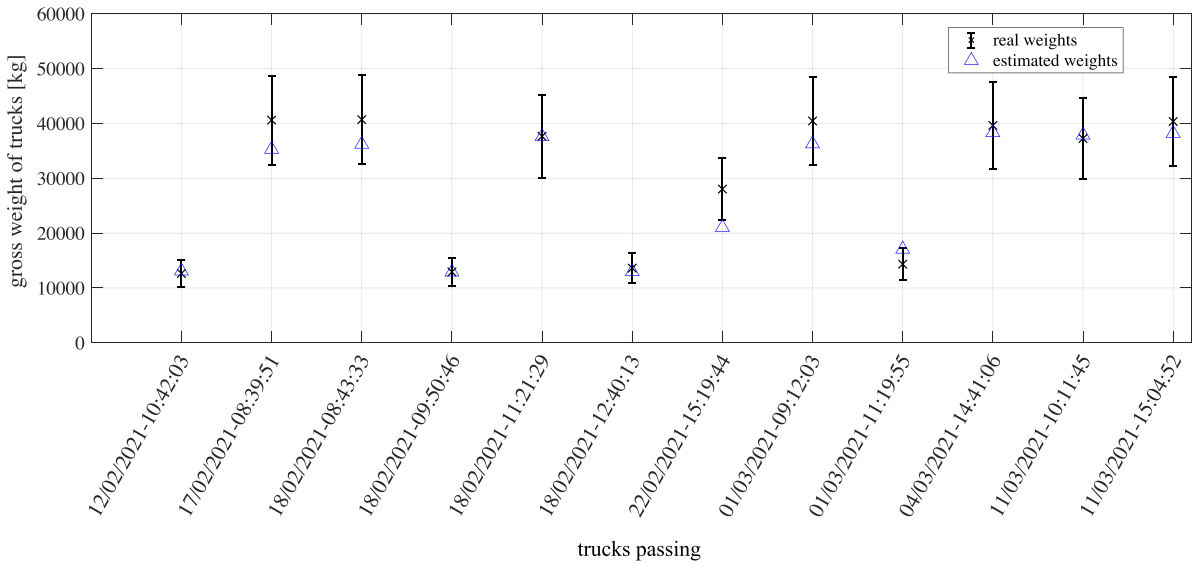

Figure 17. Weight estimations of validation data set including log times of the detected trucks. The data points include the 20% error intervals.

by figure 17, plotted together with 20% error bars. The weight identification error includes human errors that may arise due to misalignment of the trucks to the pavement due to the unsupervised collection of data. Overall, this result appears promising, and the encountered error remains within the operating limits of the international standards defined by COST323 [62], ASTM1318E-09 [63] and NMi [64].

5. Conclusion

This paper presents the results from the field deployment of an innovative monitoring system based on a smart self-sensing pavement sensor made of a new thermoplastic polymer-based material. The developed intelligent WIM system includes a dedicated low-cost electronics and a software running vehicle identification through a machine learning strategy. The smart system has been tested in field by using vehicles and trucks having various loads. Results showed that the proposed composite self-sensing material is effective at monitoring traffic loads of different magnitudes and conducting WIM sensing. Findings from this study were as follows. (i) The electrical characteristics of the polymer composite pavement were uniform showing that the dispersion procedure for adding carbon fibers was effective for great amount of material. (ii) The low-cost DAQ systems developed for the field study and utilized for the measurements through the composite pavement sensor have been shown effective, supporting 3 V of applied voltage. This voltage level reduces the demand in terms of power consumption, and facilitates the extensive utilization of smart pavement-based traffic sensors. (iii) The load sensing pavement sensor was sensitive to a wide range of weights. The signal responses generated by the pavement sensor were proportional to the vehicle weights and repeatable in the investigated range, i.e. between 1200 and 42 000 kg. (iv) The pavement sensor was capable of generating the WIM characterization signals as theoretically expected. The noise and chattering within these signals were low with respect to the amplitudes of waveform signals generated by the vehicles. This resulted in an effective load estimation based on the proposed learning algorithm, with a limited number of standard truck passages needed for training. All the above-listed characteristics make the novel type of field sensing system highly promising for low-cost WIM applications. In particular, the proposed system is significantly more cost-efficient than existing WIM sensing technologies given that DAQ system is designed at prototyping level at a price of 50 USD and the sensing material costs are comparable to the common asphalt materials. Moreover, the proposed system can estimate the weights of the measured factory trucks with an error lower than 20%, which corresponds to the standard requirement in field applications and is the recommended limit of international standards. With these findings, the proposed system is found suitable for field applications, and further tests on operating roads will allow to optimize its design over realistic operating conditions, including faster vehicle speeds and different sets of vehicle types.

Data availability statement

The data that support the findings of this study are available upon reasonable request from the authors.

Acknowledgments

This research has received funding from the European Union's Horizon 2020 research and innovation programme under Grant Agreement No. 765057 (SAFERUP! project). The authors also would like to acknowledge the contributions of Padana Resine s.r.l leading these results.

Conflict of interest

The authors declare that they have no conflict of interest.

ORCID iDs

Antonella D'Alessandro https://orcid.org/0000-0003-2928-1961
Filippo Ubertini https://orcid.org/0000-0002-5044-8482

References

[1] Zhang W and Wang N 2017 Bridge network maintenance prioritization under budget constraint *Struct. Saf.* **67** 96–104
[2] Micu E A *et al* 2019 Evaluation of the extreme traffic load effects on the forth road bridge using image analysis of traffic data *Adv. Eng. Softw.* **137** 102711
[3] Tan J S, Elbaz K, Wang Z F, Shen J S and Chen J 2020 Lessons learnt from bridge collapse: a view of sustainable management *Sustainability* **12** 1205
[4] Smirnova O, Kharitonov A and Belentsov Y 2019 Influence of polyolefin fibers on the strength and deformability properties of road pavement concrete *J. Traffic Transp. Eng.* **6** 407–17
[5] Fathalla E, Tanaka Y and Maekawa K 2018 Remaining fatigue life assessment of in-service road bridge decks based upon artificial neural networks *Eng. Struct.* **171** 602–16
[6] Pai S G, Nussbaumer A and Smith I F 2018 Comparing structural identification methodologies for fatigue life prediction of a highway bridge *Front. Built Environ.* **3** 73
[7] Yan W, Deng L, Zhang F, Li T and Li S 2019 Probabilistic machine learning approach to bridge fatigue failure analysis due to vehicular overloading *Eng. Struct.* **193** 91–99
[8] Yuan M, Liu Y, Yan D and Liu Y 2019 Probabilistic fatigue life prediction for concrete bridges using Bayesian inference *Adv. Struct. Eng.* **22** 765–78
[9] Contreras-Nieto C, Shan Y, Lewis P and Hartell J A 2019 Bridge maintenance prioritization using analytic hierarchy process and fusion tables *Autom. Constr.* **101** 99–110
[10] Mandić Ivanković A, Skokandić D, Žnidarič A and Kreslin M 2019 Bridge performance indicators based on traffic load monitoring *Struct. Infrastruct. Eng.* **15** 899–911
[11] Wu C, Wu P, Wang J, Jiang R, Chen M and Wang X 2020 Critical review of data-driven decision-making in bridge operation and maintenance *Struct. Infrastruct. Eng.* **18** 1–24
[12] Mao X, Jiang X, Yuan C and Zhou J 2020 Modeling the optimal maintenance scheduling strategy for bridge networks *Appl. Sci.* **10** 498
[13] Farreras-Alcover I, Chryssanthopoulos M K and Andersen J E 2017 Data-based models for fatigue reliability of orthotropic steel bridge decks based on temperature, traffic and strain monitoring *Int. J. Fatigue* **95** 104–19
[14] Lu N, Liu Y and Deng Y 2019 Fatigue reliability evaluation of orthotropic steel bridge decks based on site-specific weigh-in-motion measurements *Int. J. Steel Struct.* **19** 181–92
[15] Ye Z, Ji B H, Yuanzhou Z and Fu Z Q 2020 Investigation of the fatigue vehicle load for a long-span steel bridge based on nine years of measured traffic data *Struct. Eng. Int.* 1–9
[16] Sekiya H, Kimura K and Miki C 2016 Technique for determining bridge displacement response using MEMS accelerometers *Sensors* **16** 257
[17] Di J, Ruan X, Zhou X, Wang J and Peng X 2021 Fatigue assessment of orthotropic steel bridge decks based on strain monitoring data *Eng. Struct.* **228** 111437
[18] Bertolesi E, Buitrago M, Adam J M and Calderón P A 2021 Fatigue assessment of steel riveted railway bridges: full-scale tests and analytical approach *J. Constructional Steel Res.* **182** 106664
[19] Nagulapally P, Shamsuddoha M, Rajan G, Mohan M and Prusty B G 2021 Distributed fiber optic sensor-based strain monitoring of a riveted bridge joint under fatigue loading *IEEE Trans. Instrum. Meas.* **70** 6009610
[20] Ma Y, Wang G, Guo Z, Wang L, Jiang T and Zhang J 2019 Critical region method-based fatigue life prediction of notched steel wires of long-span bridges *Constr. Build. Mater.* **225** 601–10
[21] Lee J, Lee K C, Cho S and Sim S H 2017 Computer vision-based structural displacement measurement robust to light-induced image degradation for in-service bridges *Sensors* **17** 2317
[22] Khuc T and Catbas F N 2018 Structural identification using computer vision–based bridge health monitoring *J. Struct. Eng.* **144** 04017202
[23] Vicente M A, Gonzalez D C, Minguez J and Schumacher T 2018 A novel laser and video-based displacement transducer to monitor bridge deflections *Sensors* **18** 970
[24] Luo L, Feng M Q and Wu Z Y 2018 Robust vision sensor for multi-point displacement monitoring of bridges in the field *Eng. Struct.* **163** 255–66
[25] Feng D and Feng M Q 2017 Experimental validation of cost-effective vision-based structural health monitoring *Mech. Syst. Signal Process.* **88** 199–211
[26] Hou S and Wu G 2019 A low-cost IoT-based wireless sensor system for bridge displacement monitoring *Smart Mater. Struct.* **28** 085047
[27] Sony S, Laventure S and Sadhu A 2019 A literature review of next-generation smart sensing technology in structural health monitoring *Struct. Control Health Monit.* **26** e2321
[28] Yin Y, Fang Z, Liu Y and Han F 2019 Temperature-insensitive structure design of micromachined resonant accelerometers *Sensors* **19** 1544
[29] Han Q, Ma Q, Xu J and Liu M 2021 Structural health monitoring research under varying temperature condition: a review *J. Civil Struct. Health Monit.* **11** 149–73
[30] Noel A B, Abdaoui A, Elfouly T, Ahmed M H, Badawy A and Shehata M S 2017 Structural health monitoring using wireless sensor networks: a comprehensive survey *IEEE Commun. Surv. Tutorials* **19** 1403–23
[31] Yang Z and Pun-Cheng L S 2018 Vehicle detection in intelligent transportation systems and its applications under varying environments: a review *Image Vis. Comput.* **69** 143–54
[32] Dong H, Wang X, Zhang C, He R, Jia L and Qin Y 2018 Improved robust vehicle detection and identification based on single magnetic sensor *IEEE Access* **6** 5247–55
[33] Garcia F, Martin D, De La Escalera A and Armingol J M 2017 Sensor fusion methodology for vehicle detection *IEEE Int. Transp. Sys. Mag.* **9** 123–33
[34] Felguera-Martín D, González-Partida J T, Almorox-González P and Burgos-García M 2012 Vehicular traffic surveillance and road lane detection using radar interferometry *IEEE Trans. Veh. Technol.* **61** 959–70
[35] Croce P 2001 Background to fatigue load models for Eurocode 1: Part 2 Traffic Loads *Prog. Struct. Eng. Mater.* **3** 335–45
[36] Sujon M and Dai F 2021 Application of weigh-in-motion technologies for pavement and bridge response monitoring: state-of-the-art review *Autom. Constr.* **130** 103844
[37] Birgin H B, Laflamme S, D'Alessandro A, Garcia-Macias E and Ubertini F 2020 A weigh-in-motion characterization algorithm for smart pavements based on conductive cementitious materials *Sensors* **20** 659

[38] Richardson J, Jones S, Brown A, O'Brien E and Hajializadeh D 2014 On the use of bridge weigh-in-motion for overweight truck enforcement *Int. J. Heavy Veh. Syst.* **21** 83–104
[39] Iatsko O, Babu A R, Stallings J M and Nowak A S 2020 Weigh-in-motion-based fatigue damage assessment *Transp. Res. Rec.* **2674** 710–9
[40] Hou R, Dedhia Y A, Jeong S, Law K, Ettouney M and Lynch J P 2019 Fusion of weigh-in-motion system and bridge monitoring data for bridge load rating *Proc. 9th Int. Conf. on Structural Health Monitoring of Intelligent Infrastructure (St. Louis, MO)* pp 4–7
[41] Jacob B and Feypell-de L B V 2010 Improving truck safety: potential of weigh-in-motion technology *IATSS Res.* **34** 9–15
[42] Kwon T M 2016 Implementation and evaluation of a low-cost weigh-in-motion system Center for Transportation Studies, University of Minnesota
[43] Yu Y, Cai C and Deng L 2018 Nothing-on-road bridge weigh-in-motion considering the transverse position of the vehicle *Struct. Infrastruct. Eng.* **14** 1108–22
Han B, Zhang K, Yu X, Kwon E and Ou J 2011 Nickel particle-based self-sensing pavement for vehicle detection *Measurements* **44** 1645–50
[45] Han B, Zhang K, Burnham T, Kwon E and Yu X 2012 Integration and road tests of a self-sensing CNT concrete pavement system for traffic detection *Smart Mater. Struct.* **22** 015020
[46] Han B, Yu X and Kwon E 2009 A self-sensing carbon nanotube/cement composite for traffic monitoring *Nanotechnology* **20** 445501
[47] Pan P, Wu S, Xiao F, Pang L and Xiao Y 2015 Conductive asphalt concrete: a review on structure design, performance and practical applications *J. Intell. Mater. Syst. Struct.* **26** 755–69
[48] D'Alessandro A, Birgin H B and Ubertini F 2021 Advanced monitoring of structures and infrastructures through smart composite sensors and systems *Civil Structural Health Monitoring (Lecture Notes in Civil Engineering)* vol 156 (Switzerland: Springer) pp 485–98
[49] Downey A, D'Alessandro A, Ubertini F and Laflamme S 2018 Automated crack detection in conductive smart-concrete structures using a resistor mesh model *Meas. Sci. Technol.* **29** 035107
[50] Birgin H B, D'Alessandro A, Laflamme S and Ubertini F 2021 Hybrid carbon microfibers-graphite fillers for piezoresistive cementitious composites *Sensors* **21** 518
[51] Birgin H B, D'Alessandro A, Laflamme S and Innovative Carbon-Doped U F 2021 Composite pavements with sensing capability and low environmental impact for multifunctional infrastructures *J. Compos. Sci.* **5** 192
[52] Raspberry Pi Foundation 2022 Raspberry pi documentation (available at: www.raspberrypi.com/documentation/computers/raspberry-pi.html#raspberry-pi-zero) (Accessed 14 April 2022)
[53] Texas Instruments 2018 ADS1115 technical datasheet (available at: www.ti.com/lit/ds/symlink/ads1114.pdf?ts=1649901729629) (Accessed 14 April 2022)
[54] Arduino 2022 Arduino nano (available at: https://docs.arduino.cc/hardware/nano) (Accessed 14 April 2022)
[55] Choi J Y, Krstic M, Ariyur K B and Lee J S 2002 Extremum seeking control for discrete-time systems *IEEE Trans. Autom. Control* **47** 318–23
[56] Alpaydin E 2014 *Introduction to Machine Learning (Adaptive Computation and Machine Learning Series)* (Cambridge: MIT Press)
[57] Corecom 2016 EVIzero technical data sheet (available at: www.evizero.com/download/technical-standards-of-contract-rev-01.pdf) (Accessed 14 April 2022)
[58] SGL Carbon 2022 Sigrafil short carbon fibers (available at: www.sglcarbon.com/en/markets-solutions/material/sigrafil-short-carbon-fibers) (Accessed 14 April 2022)
[59] Pan N 1993 A modified analysis of the microstructural characteristics of general fiber assemblies *Text. Res. J.* **63** 336–45
[60] Kumar V and Rawal A 2016 Tuning the electrical percolation threshold of polymer nanocomposites with rod-like nanofillers *Polymer* **97** 295–9
[61] García-Macías E, D'Alessandro A, Castro-Triguero R, Pérez-Mira D and Ubertini F 2017 Micromechanics modeling of the uniaxial strain-sensing property of carbon nanotube cement-matrix composites for SHM applications *Compos. Struct.* **163** 195–215
[62] Jacob B 1995 European research activity cost-323: weigh-in-motion of road vehicles *1st European Conf. on Weigh-in-Motion of Road Vehicles (Zurich, 8–10 March 1995)*
[63] US department of transportation federal highway administration office of highway policy information 2018 Weigh-in-motion pocket guide part 1: WIM technnology, data acquisition, and procurement guide (available at: www.fhwa.dot.gov/policyinformation/knowledgecenter/wim_guide/wim_guidebook_part1_070918_(508_compliant).pdf) (Accessed 15 December 2021)
[64] NMi Certin 2016 NMi Int. WIM standard specifications and test procedures weigh-in-motion systems (available at: www.is-wim.net/wp-content/uploads/2020/10/NMi-Int.-WIM-Standard-V1.0-ICWIM-7-Scientific-Committee-SIGNED.pdf) (Accessed 15 December 2021)